Earth and Planetary Science
https://journals.nasspublishing.com/index.php/eps

RESEARCH ARTICLE

Discovery of the Naturally Occurring Pure $CaTiO_3$ Cubic Perovskite from Tazheran Massif

Jing Sun[1,2*], Jin Liu[3], Fuyang Liu[3], Eugene Sklyarov[4], Ross N. Mitchell[5]

1. State Key Laboratory of Petroleum Resources and Prospecting, China University of Petroleum, Beijing, 102249, China
2. College of Geoscience, China University of Petroleum, Beijing, 102249, China
3. Center for High Pressure Science and Technology Advanced Research, Beijing, 102249, China
4. Institute of the Earth's Crust, Siberian Branch of the Russian Academy of Sciences, Irkutsk, 664033, Russia
5. Institute of Geology and Geophysics, Chinese Academy of Sciences, Beijing, 100029, China

Abstract: As the parent compound of the perovskite-structured family and an analogue of davemaoite $CaSiO_3$ in Earth's lower mantle, $CaTiO_3$ perovskite is widely used in electronic ceramic materials, immobilizing radioactive waste, and geosciences. Here we report the discovery of a natural pure $CaTiO_3$ perovskite-*C* in calc-silicate veins in brucite marble in the Tazheran Massif, Russia. The mean composition of perovskite-*C* is 97 wt% total CaO and TiO_2, and minor impurities of Na, Al, and Zr, yielding the chemical formula $CaTi_{0.97}Al_{0.01}Na_{0.01}Zr_{0.01}O_3$. The cubic crystal structure—$Pm\bar{3}m$, $Z = 1$: a = 3.8301 Å, V = 56.19 (2) Å^3 (ρ = 4.019 g/cm^3) has been refined to R_1 = 0.0451. Compared with the cubic perovskite discovered in Israel, the cubic perovskite discovered in this study is very pure in Ca and Ti. The naturally occurring perovskite-*C* from Tazheran implies that the host skarn might have experienced high-temperature (> 1247–1374 °C) metamorphism and/or metasomatism at an early stage. Moreover, the discovery of natural perovskite-C also draws attention to considering crystal-structure-related matrix effects in the future of in situ U-Pb geochronology, especially using Tazh international perovskite standards.

Keywords: Perovskite; Cubic crystal structure; $CaTiO_3$; SCXRD; Tazheran Massif

*Corresponding Author:
Jing Sun,
State Key Laboratory of Petroleum Resources and Prospecting, China University of Petroleum, Beijing 102249, China; Colleage of Geoscience, China University of Petroleum, Beijing, 102249, China;
Email: sunjing@cup.edu.cn

Received: 23 November 2023; **Received in revised form:** 14 March 2024; **Accepted:** 7 April 2024; **Published:** 25 April 2024

Citation: Sun, J., Liu, J., Liu, F., et al., 2024. Discovery of the Naturally Occurring Pure $CaTiO_3$ Cubic Perovskite from Tazheran Massif. *Earth and Planetary Science*. 3(1): 35–43. DOI: https://doi.org/10.36956/eps.v3i1.991

DOI: https://doi.org/10.36956/eps.v3i1.991

1. Introduction

Perovskite was originally discovered in 1839 by Gustav Rose in the Ural Mountains, Russia [1], and named after a Russian mineralogist, Lev Aleksevich von Perovski (1792–1856). As the parent compound of the perovskite-structured family [2], perovskite is widely used in electronic ceramic materials and for immobilizing high-level radioactive waste [3–5]. Additionally, perovskite is an appropriate analogue for davemaoite $CaSiO_3$ in Earth's lower mantle [6,7] and thus it also plays an important role in geoscience [8].

The ideal perovskite structure is cubic [9–13]. However, due to the large size of cations, Ca and Ti are easily replaced by other cations [5,12]. Ca could be substituted by Na^+, Sr^{2+}, K^+, Pb^{2+}, REE^{3+}, and Ba^{2+}, while Ti could be replaced by Fe^{3+}, Fe^{2+}, Nb^{5+}, Th^{4+}, Ta^{5+}, and Zr^{4+}. Hence, the majority of natural perovskite grains are unlikely to be pure, and their crystal structures are orthorhombic [5,12,14]. Even for synthetic pure perovskite crystals in experiments, the perovskite-*C* ($CaTiO_3$ perovskite with cubic structure) is not observed until the temperature is increased to > 1247–1374 °C [2,15–18] The naturally occurring $CaTiO_3$ perovskite (No. 1011211) was first reported to be cubic $Pm\bar{3}m$ by Barth [19] but the precision of the method used to confirm the crystal structure nearly a century ago is open to question. The X-ray diffraction techniques used then, for example, could not have distinguished orthorhombic and tetragonal $CaTiO_3$ from cubic, which may have resulted in a false positive. Recently, natural cubic perovskite $Ca(Ti, Si, Cr)O_3$ was found in a pyrometamorphic complex in Israel [20]. However, the cubic perovskite discovered in Israel contains very high SiO_2 contents (8.12 wt%) and Cr_2O_3 (60.2 wt%), and the pure $CaTiO_3$ cubic perovskite has never been discovered.

This contribution presents the discovery of a naturally occurring perovskite-*C* in the Tazheran Massif, Russia, using both Raman and single crystal X-ray diffraction (SCXRD). The natural perovskite-*C* carries implications not only for the geological history of the Tazheran Massif but also for *in situ* perovskite U-Pb geochronology that commonly uses perovskite of the Tazheran Massif as a standard.

2. Occurrence and Analytical Methods

The perovskite-*C* (N52°50'11.15", E106°43'22.11") in this study was collected in the Tazheran Massif, Russia. The Tazheran Massif is an area of 6 km^2 along the western shore of Lake Baikal, which is a part of the Olkhone terrane within the Early Paleozoic Baikal accretionary-collisional belt on the southern margin of the Siberian craton [21]. The Massif is composed of syenite, nepheline syenite, and subalkaline gabbro, with numerous bodies of brucite marble of various sizes and shapes. It has been well-known for Tazheran Massif mineralogists since the beginning of the latter half of the 20th century for several new minerals being discovered, such as tazheranite and azoproite.

Two main types of $CaTiO_3$-bearing metasomatic rocks occurred in the Tazheran Massif: skarn-related forsterite-spinel calc-silicate veins in brucite marble and skarns at the contact of nepheline syenite with brucite marble [21]. The crystal structure of perovskite grains (Tazh-3) in the nepheline syenite veins are orthorhombic, and its crystal structure and chemical compositions have been reported by Sun et al. [22], whereas the perovskite-*C* (Tazh-1) documented here occurs in the calc-silicate veins in brucite marble. The calc-silicate veins are irregular in shape, varying in thickness from several cm to 1 meter, and they are dominantly composed of forsterite, Ti-bearing spinel, and calcite with less abundant clinohumite and dolomite [21]. The perovskite-*C*, tazheranite, calzirtite, geikielite, and Mg-bearing ilmenite are accessory minerals. The occurrence of perovskite-*C* is unevenly distributed in calc-silicate rocks with crystal grains 1 to 3 mm in diameter, and the largest crystal grain is up to 2 cm [21].

One perovskite crystal grain was randomly selected from sample Tazh-1. The crystal grain was placed on a glass slide and covered with epoxy resin in a cylindrical frame. The surface of this side was polished for further X-ray fluorescence (XRF) and back-scattered electron (BSE) images at the Institute of Geology and Geophysics, Chinese Academy of Sciences (IGGCAS). The XRF instrument is a Bruker M4 PLUS Micro-XRF with two SDD detectors, the high voltage is 50 kV with 500 μA anode current, and the pixel size is 8 μm. The chemical compositions of six Tazh-1 perovskite crystal grains were measured by electron probe micro-analyzer (EPMA) using a JEOL JXA-8100 electron microprobe as well as BSE images at IGGCAS. A variety of natural and synthetic standards were used to calibrate the major components, some of which were also measured as unknowns to monitor data quality. The ZAF model [23] was applied for matrix correction. The analytical uncertainties for EPMA are within 2% for TiO_2 and CaO, but 10–20% for other elements due to their low concentrations. The grains were crushed into small pieces and then hand-picked under a binocular microscope for pure euhedral pieces without inclusions and sawtooth rims.

A piece of perovskite 40 μm in size was analyzed us-

ing SCXRD. Diffraction data were collected on a Bruker D8 Venture Photo II diffractometer equipped with a Microfocus Incoatec Mo K_α radiation and a multilayer optic monochromator at the Center for High-Pressure Science and Technology Advanced Research (HPSTAR). A total of 436 frames were collected. The total exposure time was 0.12 hours. The frames were integrated with the Bruker SAINT software package using a narrow-frame algorithm. Data were corrected for absorption effects using the Multi-Scan method (SADABS). The ratio of minimum to maximum apparent transmission was 0.553. The structure was refined using the Bruker SHELXTL Software Package, to the space group $Pm\bar{3}m$, with Z = 1 for the equation unit $CaTiO_3$. Crystallographic data for the structures reported here have been deposited with the Cambridge Crystallographic Data Centre (CCDC), which contains the supplementary crystallographic data for this paper (https://www.ccdc.cam.ac.uk/structures/). These data can be obtained free of charge from The Cambridge Crystallographic Data Centre via www.ccdc.cam.ac.uk/structures. This report and the CIF file were generated using FinalCif.

Perovskite crystal grains from both nepheline syenite (Tazh-3) and calc-silicate (Tazh-1) veins were randomly selected for laser Raman analysis. It was carried out at the Beijing SHRIMP Center using the Horiba LabRam HR Evolution integrated LabSpec6 software. Analyses on perovskite surfaces were carried out using a Laser Quantum 532 nm (110 mW) and 100 × objective lens under ambient conditions. The spectra were collected in the Raman band range of 200–900 cm^{-1}. Based on the equation spatial resolution of spot analysis = 0.61 λ/NA (λ = 532 nm, NA = 0.9), the spatial resolution of spot analysis was 0.721 μm. Multichannel spectra were typically acquired after three accumulations using a 15-second integration time. Before analysis, the grating turret accuracy was calibrated between the zero-order line and laser line at 0 cm^{-1}. Spectral accuracy was verified on the silicon peak, which always lies within three detector pixels around the theoretical value (520.7 cm^{-1}). After analysis, baseline corrections and peak fitting were carried out by Lorentzian amplitude functions.

3. Results and Discussion

The chemical composition of the perovskite-*C* (Tazh-1) is very homogeneous, without compositional zones of Ca and Ti as seen in both BSE and XRF images (Figure 1). The perovskite-*C* determined by electron microprobe analysis in this study is especially pure $CaTiO_3$, with nearly 97 wt% total CaO (40.88%) and TiO_2 (56.32%), and the trace elements are no more than 4 wt% in total: 0.28 wt% Al_2O_3, 0.18 wt% Na_2O, 0.45 wt% ZrO_2, 0.22 wt% FeO, 0.76 wt% REE_2O_3, and 0.30 wt% Nb_2O_5 (Table 1). To check for anion deficiency in our sample of the perovskite-*C*, microprobe data were normalized to a cation-site sum of 2.0 and compared to the formulas generated by normalizing to an O-site sum of 3.0 (Table 1). The equation is $CaTi_{0.97}Al_{0.01}Na_{0.01}Zr_{0.01}O_3$, with minor impurities of Na, Al, and Zr totaling 0.03 atoms per formula unit. Compared with the perovskite-*C* that occurred in Israel [20], the perovskite-*C* in this study is purer (CaO + TiO_2 contents 97% vs. 80.5%) in compositions.

Raman spectrum (Figure 2) shows that Tazh-3 has a similar Raman shape as reference orthorhombic perovskite, indicating the same crystal structure. However, the Raman spectrum of perovskite-*C* (Tazh-1) is different from orthorhombic perovskite. The prominent band at 796 cm^{-1} correlates with the strongest peaks in the spectra of orthorhombic perovskite (820 cm^{-1}) and cubic perovskite in a previous study (797 cm^{-1}) [20]. It has been suggested that the 796 cm^{-1} band in the spectrum of perovskite-C represent the B-site, i.e., Ti^{4+}. The evident difference between Tazh-1 and cubic perovskite in Britvin et al. [20] study is that the Tazh-1 perovskite has many bands from 224–635 cm^{-1}. Tazh-3 and naturally occurring orthorhombic perovskite also show a few bands at 236 cm^{-1}, 271 cm^{-1} and 547 cm^{-1}, but do not have bands at 300–500 cm^{-1}. Generally, the difference in the Raman spectra could be due to four reasons: (1) Different instruments used, for example, with different spectra resolution. However, both Tazh-1 and Tazh-3 samples were analyzed in the same instrument with the same spectra resolution. (2) High impurity content may lead to the widening of peaks, and the close peaks cannot be resolved for some natural perovskites at low spectral resolution. However, the chemical compositions and BSE images indicate that Tazh-1 and Tazh-3 are pure without impurity content. (3) High concentrations of U and Th may alpha damage the crystal lattice of some natural perovskite, which also leads to peak widening [24]. And Tazh-3 and Tazh-1 have different U and Th contents (4298 ppm vs. 516 ppm U contents and 4784 ppm vs. 281 ppm Th contents [22]). Hence, different U and Th contents can explain the different Raman spectra for Tazh-1 and Tazh-3 rather than special Raman spectra for Tazh-1 with very low U and Tazh-1. (4) Different structure. In order to know the structure of Tazh-1 and Tazh-3, the SCXRD were analyzed. The integration of the diffraction data from SCXRD using the ideal cubic unit cell with the space group $Pm\bar{3}m$ yielded a total of 300 reflections to a maximum angle θ of 29.98 (0.71 Å resolution). The final cell constants of a = 3.8168 (6) Å, V = 55.60 (3) $Å^3$,

are based upon the refinement of the XYZ-centroids of 900 reflections above 20 σ (I) with 10.68 < 2θ < 60.18. The single crystal X-ray diffraction pattern is shown in Figure 3. The cell constants of perovskite-*C* in this study are similar to the perovskite-*C* (a = 3.808 (1) Å, V = 55.21 (4) Å^3) discovered in Israel [20]. The final anisotropic full-matrix least-squares refinement on F^2 with 6 variables converged at R_1 = 4.51%, for the observed data and wR_2 = 8.97% for all data. The goodness of fit was 1.425. On the basis of the final model, the calculated density was 4.019 g/cm^3 (Table 2). In the module of the perovskite-*C*, the Ca-site cation is surrounded by 12 O in twelve-fold cubo-octahedral coordination, and the Ti-site cation is surrounded by 6 O anions in octahedral coordination. The O anion is coordinated by two Ti-site and four Ca-site cations.

Table 1. Results of the chemical analysis of the Tazh-1 $CaTiO_3$ analyzed by EPMA.

Sample	Tazh-1 01	Tazh-1 02	Tazh-1 03	Tazh-1 05	Tazh-1 06	Tazh-1 09	Ave. (wt%)	Stand. Dev.	Tazh-3 Ave.	Cubic Perovskite from Isreal
CaO	40.90	41.16	41.21	41.01	40.87	40.15	40.88	0.38	37.2	42.45
TiO_2	55.87	56.66	56.22	56.17	56.32	56.66	56.32	0.30	52.6	38.08
Al_2O_3	0.30	0.22	0.30	0.41	0.22	0.21	0.28	0.08	0.45	1.21
Na_2O	0.11	0.09	0.20	0.17	0.24	0.28	0.18	0.07	0.70	
ZrO_2	0.70	0.45	0.28	0.24	0.52	0.51	0.45	0.17	0.35	
FeO	0.37	0.12	0.18	0.10	0.30	0.27	0.22	0.11	1.31	1.40
SiO_2	0.03	0.03	0.01	0.03	0.03	0.05	0.03	0.01	0.01	8.12
MnO	0.00	0.02	0.04	0.03	0.00	0.00	0.02	0.02	0.03	
MgO	0.07	0.03	0.00	0.01	0.10	0.10	0.05	0.04	0.02	0.38
P_2O_5	0.05	0.04	0.02	0.04	0.01	0.04	0.03	0.01	0.03	0.84
La_2O_3	0.09	0.09	0.09	0.11	0.19	0.18	0.13	0.05	0.53	
Ce_2O_3	0.53	0.25	0.38	0.37	0.44	0.67	0.44	0.15	1.90	
Nd_2O_3	0.19	0.08	0.18	0.18	0.14	0.32	0.18	0.08	0.79	
Nb_2O_5	0.23	0.40	0.27	0.17	0.19	0.51	0.30	0.13	1.47	
Ta_2O_5	0.00	0.00	0.02	0.00	0.01	0.00	0.01	0.01	0.02	
SrO	0.00	0.00	0.02	0.00	0.00	0.02	0.01	0.01	0.01	
Total	99.42	99.63	99.42	99.04	99.58	99.97	99.51	0.31	97.4	
Cations (O = 3)										
Ca	1.01	1.01	1.01	1.01	1.00	0.98	1.00	0.01		
Ti	0.97	0.97	0.97	0.97	0.97	0.97	0.97	0.00		
Al	0.01	0.01	0.01	0.01	0.01	0.01	0.01	0.00		
Na	0.00	0.00	0.01	0.01	0.01	0.01	0.01	0.00		
Zr	0.01	0.00	0.00	0.00	0.01	0.01	0.01	0.00		
Fe	0.01	0.00	0.00	0.00	0.01	0.01	0.00	0.00		
Si	0.00	0.00	0.00	0.00	0.00	0.00	0.00	0.00		
Mn	0.00	0.00	0.00	0.00	0.00	0.00	0.00	0.00		
Mg	0.00	0.00	0.00	0.00	0.00	0.00	0.00	0.00		
P	0.00	0.00	0.00	0.00	0.00	0.00	0.00	0.00		
La	0.00	0.00	0.00	0.00	0.00	0.00	0.00	0.00		
Ce	0.00	0.00	0.00	0.00	0.00	0.01	0.00	0.00		
Nd	0.00	0.00	0.00	0.00	0.00	0.00	0.00	0.00		
Nb	0.00	0.00	0.00	0.00	0.00	0.01	0.00	0.00		
Ta	0.00	0.00	0.00	0.00	0.00	0.00	0.00	0.00		
Sr	0.00	0.00	0.00	0.00	0.00	0.00	0.00	0.00		
Total	2.02	2.01	2.02	2.02	2.02	2.01	2.01	0.00		

Source: Britvin et al. [20], Sun et al. [22].

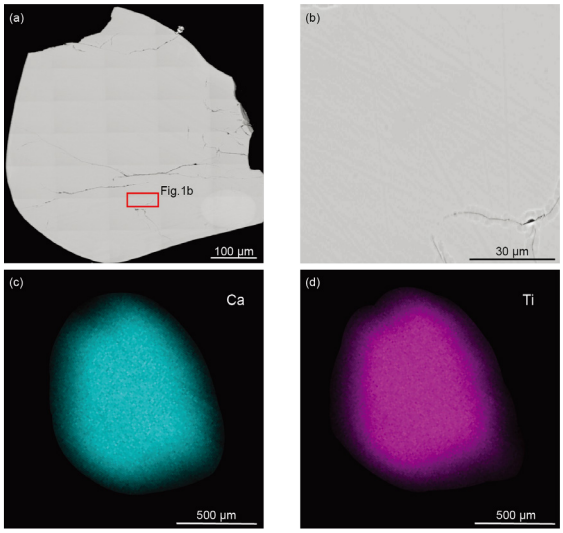

Figure 1. Back-scattered-electron (BSE) image of Tazh-1 $CaTiO_3$ and energy-dispersive X-ray spectroscopy elemental maps. (**a, b**) BSE image of the Tazh-1 $CaTiO_3$. (**c, d**) Energy-dispersive X-ray spectroscopy elemental maps of Ca (**c**) and Ti (**d**). The colour intensity is proportional to the element concentration.

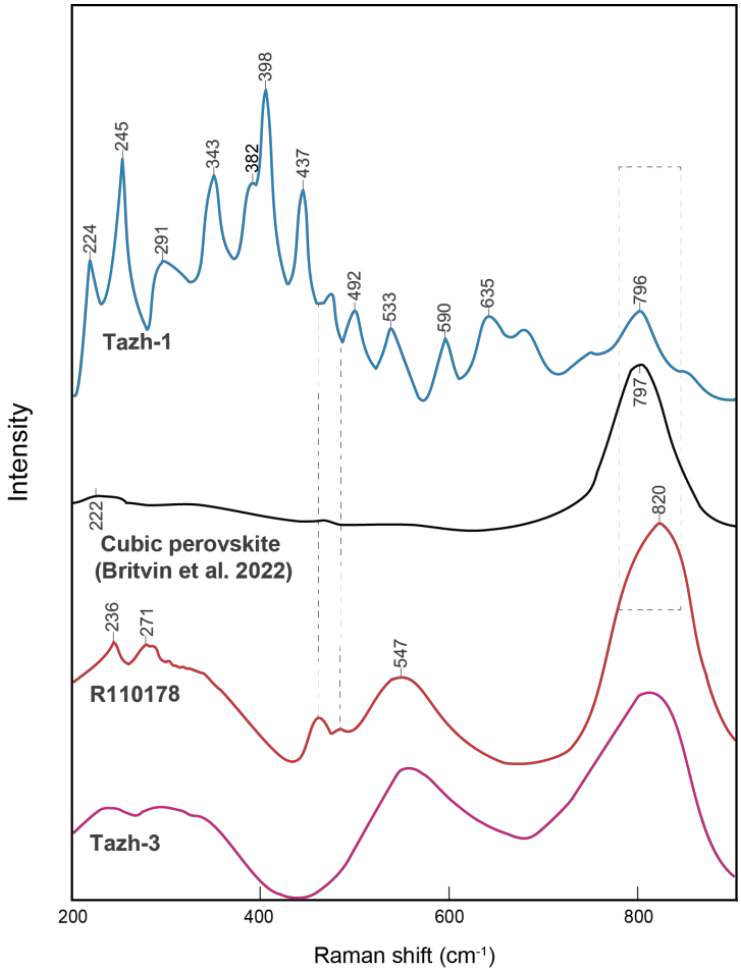

Figure 2. Raman spectroscopy results of Tazh-1 and Tazh-3 perovskite grains. Baseline-corrected Raman spectrum of the Ca-Pv inclusion compared with that of the $CaTiO_3$-perovskite intergrowth. R110178 data is from the RRUFF database (https://rruff.info/). Cubic perovskite is from source: Britvin et al. [20].

Table 2. Summary of crystal data and refinement results for Tazh-1 $CaTiO_3$.

		Tazh-1
CCDC number		2340711
Chemical formula		$CaTi_{0.97}Al_{0.01}Na_{0.01}Zr_{0.01}O_3$
Temperature		296(2) K
Space group		$Pm\bar{3}m$
Equation weight		135.98 g/mol
Wave length (Å)		0.71073
a (Å)		3.8168(6)
Volume ($Å^3$)		55.60(3)
Z		1
2θ range for data collection		10.68°–60.18°
Density (calculated, g/cm^3)		4.061
Absorption coefficient (mm^{-1})		5.841
No. of reflections collected		289
No. of independent reflections		32
Final R_1, wR_2 factors [$I > 2\sigma(I)$]		0.0431, 0.0844
Final R_1, wR_2 factors (all data)		0.0568, 0.0950
Goodness of fit		1.258
Largest peak/jole Ca		0.72/–0.81
	x	0
	y	0
	z	0
	U(eq)	0.0264(17)
Ti	*x*	–0.5
	y	0.5
	z	0.5
	U(eq)	0.0110(14)
O	*x*	–0.5
	y	0.5
	z	0
	U(eq)	0.082(7)

Figure 3. Full spectrum of a single-crystal X-ray diffraction of Tazh-1 $CaTiO_3$.

4. Implications

Chemically, the natural perovskite-*C* from the Tazheran Massif is close to pure synthetic perovskite from high-temperature/pressure experiments. Synthetic perovskite is orthorhombic in structure at room temperature and it transforms to the cubic phase at temperatures exceeding 1247–1374 °C [2,15–18]. High-pressure experiment suggests that no perovskite-*C* was observed upon compression to 44.5 GPa at room temperature [25]. Different from the perovskite-*C* discovered in Israel [20], probably formed at high pressure, perovskite-*C* from Tazheran has neither $CaSiO_3$ and Cr_2O_3 components nor melilitic glass inclusions. Perovskite-*C* from Tazheran may be a high-temperature phase. Nevertheless, based on thermodynamic modeling, the Tazheran brucite marble formed in the range of 500–580 °C and 1–5 kbar [26]. According to Konev and Samoilov [29], the temperature of Tazheran metasomatic processes reached 850–900 °C. At such temperatures, the crystal structure of perovskite should be orthorhombic, which thus cannot account for the occurrence of both orthorhombic and perovskite-*C* in the Tazheran Massif. Most skarn deposits are typified by moderate temperatures of 600–800 °C [27], although one notable exception is the early skarn alteration stage of the Bushveld complex that might have exceeded 1200 °C [28].

Therefore, the occurrence of the naturally occurring perovskite-*C* in Tazheran may indicate that the early metamorphic and metasomatic temperatures on parts of Tazheran Massif have exceeded 1247–1374 °C. The rapid decrease in temperature processes such as uplifting and/or intruding at shallow depth makes the cubic crystal structure retained. Alternatively, the different chemical compositions may contribute to different structures. Cubic and orthorhombic perovskites in the Tazheran Massif are preserved in calc-silicate and nepheline-syenite veins, respectively. Orthorhombic perovskites in the Tazheran Massif have more rare earth elements (REEs) contents than perovskite-*C* in this study [21]. REE^{3+} substituted Ca^{2+} would result in the tilting of TiO_6 octahedral units along the *Z* axis, and decreasing the length of the crystal axis [29,30]. Therefore, potential fluid effects on the perovskite structural phase transition thus cannot be ruled out. Further geological and petrological features of the Tazheran Massif are needed and beyond the scope of this paper.

Perovskite is widely used for U-Pb geochronology by *in situ* methods, i.e., secondary ion mass spectroscopy (SIMS) and laser ablation inductively coupled plasma mass spectroscopy (LA-ICPMS). *In situ* analyses need calibration materials (i.e., standards), which

must mimic the behavior (chemical compositions and crystal structures) in the unknowns. Previous studies on zircons and baddeleyites indicate that the chemical composition and crystal structure-related matrix effect may lead to U-Pb age offset by more than 4% [31–34]. Hence, perovskite U-Pb data analyzed by those *in situ* methods may be only valid if the sample and the used standards have identical crystal structures, either orthorhombic or perovskite-*C*. To date, perovskite standards used in most of the laboratories are orthorhombic; for example, orthorhombic Tazh perovskite is an international perovskite U-Pb dating standard, which is widely used in SIMS and LA-ICPMS labs worldly. Our recent study on the U-Pb ages of Tazh-1 (Perovskite-*C*) suggested that its SIMS and LA-ICPMS ages are 8% and 3% younger than its TIMS age [22] via using the orthorhombic perovskite as standards. The discovery of the naturally occurring perovskite-*C* from Tazheran Massif not only reminds using Tazh perovskite standards with caution, but also draws attention to the importance of considering crystal-structure-related matrix effects in the future of *in situ* U-Pb geochronology.

Author Contributions

Jing Sun designed this study, prepared the manuscript and did all the analysis. Jin Liu and Fuyang Liu did an SCXRD analysis. Eugene Sklyarov applied the samples. Ross N. Mitchel designed this study and polished the manuscript. All authors have read and agreed to the published version of the manuscript.

Funding

The research was supported by the National Natural Science Foundation of China Grant 42072060.

Acknowledgments

Xiaowan Su of the Center for High-Pressure Science and Technology Advanced Research helped with SCXRD analyses. The work benefitted from discussions with Roger Mitchell, Rucheng Wang, Baoyun Wang, Junlai Liu, Yi Zhao, Guowu Li and Shan Qin.

Data Availability Statement

The CCDC data can be downloaded from https://www.ccdc.cam.ac.uk/structures/.

Conflict of Interest

The authors disclosed no conflict of interest.

References

[1] Rose, G., 1839. Description of some new minerals from the Urals. Pogendorff Annals of Physics and Chemistry. 48, 551–572. (in German).
DOI: https://doi.org/10.1002/andp.18391241205

[2] Ali, R., Yashima, M., 2005. Space group and crystal structure of the perovskite $CaTiO_3$ from 296 to 1720K. Journal of Solid State Chemistry. 178(9), 2867–2872.
DOI: https://doi.org/10.1016/j.jssc.2005.06.027

[3] Ball, C.J., Begg, B.D., Cookson, D.J., et al., 1998. Structures in the system $CaTiO_3/SrTiO_3$. Journal of Solid State Chemistry. 139(2), 238–247.
DOI: https://doi.org/10.1006/jssc.1998.7836

[4] Newnham, R.E., Ruschau, G.R., 1991. Smart electroceramics. Journal of the American Chemical Society. 74, 463–480.
DOI: https://doi.org/10.1111/j.1151-2916.1991tb04047.x

[5] Wang, R.C., Xu, S.J., Lu, J.J., et al., 2000. Crystal-chemistry and geochemistry of perovskite-group minerals. Earth Science Frontiers. 7(2), 457–465. (in Chinese).

[6] Harte, B., Hudson, N.F.C. (editors), 2013. Mineral associations in diamonds from the lowermost upper mantle and uppermost lower mantle. Proceedings of the 10th International Kimberlite Conference; 2013 Jan 1st; Bangalore, India. p 235–253.
DOI: https://doi.org/10.1007/978-81-322-1170-9_15

[7] Nestola, F., Korolev, N., Kopylova, M., et al., 2018. $CaSiO_3$ perovskite in diamond indicates the recycling of oceanic crust into the lower mantle. Nature. 555, 237–241.
DOI: https://doi.org/10.1038/nature25972

[8] Ringwood, A.E., 1962. A Model for the upper mantle: 2. Journal of Geophysical Research. 67(11), 4473–4478.
DOI: https://doi.org/10.1029/JZ067i011p04473

[9] Glazer, A.M., 1972. The classification of tilted octahedra in perovskites. Acta Crystallographica. B28, 3384–3392.
DOI: https://doi.org/10.1107/S0567740872007976

[10] Howard, C.J., Stokes, H.T., 1998. Group theoretical analysis of octahedral tilting in perovskites. Acta Crystallographica. B54, 782–789.
DOI: https://doi.org/10.1107/S0108768198004200

[11] Howard, C.J., Stokes, H.T., 2005. Structures and phase transitions in perovskites—A group theoretical approach. Acta Crystallographica. A61, 93–111.

DOI: https://doi.org/10.1107/S0108767304024493

[12] Mitchell, R.H., 2002. Perovskites: Modern and Ancient. Almaz Press Inc.: Thunder Bay, ON, Canada. pp. 318.

[13] Mitchell, R.H., Burns, P.C., Chakhmouradian, A.R., 2000. The crystal structures of loparite-(Ce). The Canadian Mineralogist. 38(1), 145–152.
DOI: https://doi.org/10.2113/gscanmin.38.1.145

[14] Mitchell, R.H., Welch, M.D., Chakhmouradian, A.R., 2017. Nomenclature of the perovskite super group: A hierarchical system of classification based on crystal structure and composition. Mineralogical Magazine. 81(3), 411–461.
DOI: https://doi.org/10.1180/minmag.2016.080.156

[15] Kennedy, B.J., Howard, C.J., Chakoumakos, B.C., 1999. Phase transitions in perovskite at elevated temperatures—a powder neutron diffraction study. Journal of Physics: Condensed Matter. 11, 1479–1488.
DOI: https://doi.org/10.1088/0953-8984/11/6/012

[16] Redfern, S.A.T., 1996. High-temperature structural phase transitions in perovskite ($CaTiO_3$). Journal of Physics: Condensed Matter. 8, 8267–8275.
DOI: https://doi.org/10.1088/0953-8984/8/43/019

[17] Vogt, T., Schmahl, W.W., 1993. The high-temperature phase transition in perovskite. Europhysics Letters. 24(4), 281–285.
DOI: https://doi.org/10.1209/0295-5075/24/4/008

[18] Wang, Y., Liebermann, R.C., 1993. Electron microscopy study of domain structure due to phase transitions in natural perovskite. Physics and Chemistry of Minerals. 20, 147–158.
DOI: https://doi.org/10.1007/BF00200117

[19] Barth, T., 1925. The crystal structure of perovskite and related compounds. Norsk Geologisk Tidsskrift. 8, 201–216. Available from: https://njg.geologi.no/publications/die-kristallstruktur-von-perowskit-und-verwandten-verbindungen/ (in German).

[20] Britvin, S.N., Vlasenko, N.S., Aslandukov, A., et al., 2022. Natural cubic perovskite, $Ca(Ti,Si,Cr)O_{3-\delta}$, a versatile potential host for rock-forming and less-common elements up to Earth's mantle pressure. American Mineralogist. 107(10), 1936–1945.
DOI: https://doi.org/10.2138/am-2022-8186

[21] Sklyarov, E.V., Karmanov, N.S., Lavrenchuk, A.V., et al., 2019. Perovskites of the Tazheran Massif (Baikal, Russia). Minerals. 9(5), 323.
DOI: https://doi.org/10.3390/min9050323

[22] Sun, J., Wu, F.Y., Sklyarov, E., et al., 2022. Matrix effects during in situ U-Pb dating of perovskite with variable crystal structure: Evidence from the Tazheran Massif, Russia. Chemical Geology. 589, 120685.
DOI: https://doi.org/10.1016/j.chemgeo.2021.120685

[23] Armstrong, J.T., 1995. CITZAF-A package of correction programs for the quantitative electron microbeam X-ray-analysis of thick polished materials, thin-films, and particles. Microbeam Analysis. 4(3), 177–200.

[24] Gautheron, C., Hueck, M., Ternois, S., et al., 2022. Investigating the shallow to mid-depth (>100–300 °C) continental crust evolution with (U-Th)/He thermochronology: a review. Minerals. 12(5), 563.
DOI: https://doi.org/10.3390/min12050563

[25] Magennis, S.W., Ferguson, A.J., Bryden, T., et al., 2003. Time-dependence of erbium(III) tris(8-hydroxyquinolate) near-infrared photoluminescence: implications for organic light-emitting diode efficiency. Synthetic Metals. 138(3), 463–469.
DOI: https://doi.org/10.1016/S0379-6779(02)00501-5

[26] Doroshkevich, A., Sklyarov, E., Starikova, A., et al., 2017. Stable isotope (C, O, H) characteristics and genesis of the Tazheran brucite marbles and skarns, Olkhon region, Russia. Mineralogy and Petrology. 111, 399–416.
DOI: https://doi.org/10.1007/s00710-016-0477-8

[27] Meinert, L.D., Dipple, G.M., Nicolescu, S., 2005. World Skarn Deposits. Society of Economic Geologists, Inc. Economic Geology 100th Anniversary. 299–336.
DOI: https://doi.org/10.5382/AV100.11

[28] Wallmach, T., Hatton, C.J., 1989. Extreme facies of contact metamorphism developed in calc-silicate xenoliths in the eastern Bushveld Complex. Canadian Mineralogist. 27(3), 509–523.

[29] Qin, S., Wang, R.C., 2004. Geometric descriptions of distorted structures of ABX_3 type perovskite and application in structural prediction. Acta Geological Sinica. 78(3), 345–351. Available from: https://www.geojournals.cn/dzxb/dzxb/article/abstract/20040345 (in Chinese).

[30] Thomas, N.W., 1998. A new global parameterization of perovskite structures. Acta Crystallographica. B54, 585–599.
DOI: https://doi.org/10.1107/S0108768198001979

[31] Black, L.P., Kamo, S.L., Allen, C.M., et al., 2004. Improved $^{206}Pb/^{238}U$ microprobe geochronology by the monitoring of a trace-element-related matrix effect; SHRIMP, ID-TIMS, ELA-ICP-MS and oxygen isotope documentation for a series of zircon standards. Chemical Geology. 205(1–2), 115–140.
DOI: https://doi.org/10.1016/j.chemgeo.2004.01.003

[32] Finch, R.J., Hanchar, J.M., Hoskin P.W.O., 2001. Rare-earth elements in synthetic zircon: Part 2. A single-crystal X-ray study of xenotime substitution. American Mineralogist. 86(5–6), 681–689. DOI: https://doi.org/10.2138/am-2001-5-608

[33] Pohlner, J.E., Schmitt, A.K., Chamberlain, K.R., et al., 2020. Baddeleyite microtextures and U-Pb discordance: insights from the Spread Eagle Intrusive Complex and Cape St. Mary's sills, Newfoundland, Canada. Geochronology Discussions. DOI: https://doi.org/10.5194/gchron-2019-21

[34] Wingate, M.T.D., Compston, W., 2000. Crystal orientation effects during ion microprobe U–Pb analysis of baddeleyite. Chemical Geology. 168(1–2), 75–97. DOI: https://doi.org/10.1016/S0009-2541(00)00184-4